Chapter 1
Magnetism

Robert L. Stamps

Abstract A summary of concepts and ideas useful for an understanding of measurable phenomena in thin film and nanostructured magnetic materials is presented. Beginning with the base definitions of magnetic moment and its relation to angular momentum, mechanisms are discussed for long range ordering based on electronic orbital overlap in insulators, and electronic band structure in metals. The nature of excitations about this ground state are also discussed, and how these can be understood by analogy to the quanta of harmonic oscillations associated with vibrations in crystals. A phenomenological model of magnetic ordering and excitations is also described, and key parameters defined in terms of symmetries allowed by the local atomic environment. Lastly, a thermodynamic view of magnetic states and configurations is summarised, and here the focus is on mechanisms for magnetic reversal and coercivity and the concepts of magnetic domain walls and domain wall mobilities are discussed.

1.1 Introduction

In this chapter we will examine magnetic phenomena arising in materials. This is a remakably rich field not only at present, but also in the past. Indeed,

Robert L. Stamps
SUPA School of Physics and Astronomy, University of Glasgow, e-mail: robert.stamps@glasgow.ac.uk

E. Beaurepaire et al. (eds.), *Magnetism and Synchrotron Radiation: Towards the Fourth Generation Light Sources*, Springer Proceedings in Physics 151,
DOI: 10.1007/978-3-319-03032-6_1,
© Springer International Publishing Switzerland 2013

William Gilbert produced one of the first great works in modern science– perhaps the first– with his book *De Magnete*. Gilbert based *De Magnete* on work he began in 1581 that some historians suggest marked the invention of the modern scientific process of experiment and hypothesis. Moreover, Gilbert recognised and noted numerous possibilities for application of magnetic materials in navigation (and also mining and military technologies). This recognition of the practical benefits that can follow from scientific research is something that permeates the field of magnetism, and continues on today.

Modern applications are fascinating because of their diversity, important because of the key technological advances they underpin, and interesting because of close linkages to fundamental problems in condensed matter research. Examples include:

- Permanent magnets: used in motors and activators, an important current materials problem is to produce low cost "super-magnets" for alternative energy production schemes;
- High density data storage and digital logic circuits: magnetic grains are used to store information, and collections of patterned, interacting magnetic particles have been proposed as basic elements in low power consumption logic circuits that can in principle approach the Landauer efficiency limit;
- Magnetic based spintronics: The Nobel Prize in 2007 was awarded in recognition of the discovery and application of ultra-sensitive magnetoresistive devices that utilise the spin dependent scattering that can exist at metallic magnetic interfaces (and which have enabled modern high density hard disk drive technologies;
- Microwave device applications: electromagnetic properties of some magnetic materials have been used for signal processing since the early days of radar, and new discoveries of how voltages and charge currents interact with magnetic moments enable entirely new types of microwave devices.

The field of magnetism is characterized by scientific research and technical applications progressing jointly. Many of recent developments will be mentioned in what follows, but the main purpose of this chapter is to provide an introduction to the essential concepts and principles underlying our understanding and descriptions of the wide variety of phenomena studied in magnetic materials. To begin, the fundamental origins of magnetic moments are discussed, along with the physical processes resulting in their possible long range orderings. Fundamental excitations and different types of dynamics exhibited by magnetic spin systems are then discussed.

Lastly, a comment on referencing is in order. This is a brief introductory summary of a large body of knowledge. A full listing of all the fine works existing would be well outside the scope of this article, and instead only a small handful of references have been included. These either reference directly research results reproduced here, or point the reader for further information to examples of relevant texts and monographs.

1.2 Magnetization and Long Range Ordering

We will be concerned exclusively with magnetic properties asociated with electrons in a material. For the most part in fact, we are concerned specifically with how a material responds magnetically to an applied magnetic field.

1.2.1 Magnetic Moment

Before talking about atoms and materials, let us first consider the behaviour of a free electron in a magnetic field $\mathbf{H} = \mathbf{B}/\mu_o$ (where $\mathbf{B}$ is the magnetic induction and μ_o is the permeability of vacuum). An electron will rotate through a circular orbit centered on $\mathbf{H}$, with frequency $\omega_c = eH/m$ where e is the charge and m is the mass of the electron. A rotating electron defines a loop of current I that encloses a circular area A. The associated magnetic moment is $\mu = IA$. Writing the current in terms of ω_c and using $A = \pi r^2$, where r is the radius of the loop, the magnetic moment is

$$\mu = -\frac{\mu_o e^2 H}{2m} r^2 \,. \tag{1.1}$$

Note that we have neglected the intrinsic spin of the electron, and will discuss this later. From this circulation of charge, we can make an important connection between magnetic moment and angular momentum. The angular momentum $\mathbf{L}$ of the circulating electron has magnitude $L = mrv$ where v is the tangential speed defined in terms of frequency as $\omega_c = v/2\pi r$. Using this with (1.1), we arrive at

$$\mu = -\frac{e}{2m}\mathbf{L} \,, \tag{1.2}$$

thereby illustrating that the magnitude of the magnetic moment is proportional to the angular momentum, and oriented oppositely.

With this in mind, we now consider the magnetic moment of electrons in atomic orbitals. Suppose that there is no field and the orbital is that of a simple Bohr model with $L = m_l\hbar$, where m_l is the Bohr angular momentum quantum number. Neglecting spin, we now expect that for $m_l = 1$,

$$\mu = \mu_B = -\frac{e\hbar}{2m} , \tag{1.3}$$

which is called the Bohr magneton.

What now is the effect of an applied magnetic field H? In the frame of reference of the electron, it turns out that H has no effect at least to first order in perturbation theory. Therefore if H is not too large, the energy is simply shifted by the amount $\hbar\omega_L$, where ω_L is the rotation frequency of the electron.

It is interesting to note that $\omega_L \neq \omega_c$. This can be seen by examining the dynamics of the atomic moment when in the presence of a field H. In order to do this, we first recall the energy and equations of motion for a moment in a magnetic field. The energy is defined as

$$E = -\mu_o \mu \cdot \mathbf{H} , \tag{1.4}$$

and the precession of angular momentum is described by the torque Γ experienced by the magnetic moment

$$\Gamma = \frac{\mathrm{d}\mathbf{L}}{\mathrm{d}t} = \mu_o \mu \times \mathbf{H} = \mu \times \mathbf{B} . \tag{1.5}$$

Placing $\mathbf{H}$ along the z direction, and assuming $\mathbf{L} = a(\hat{x} + \mathrm{i}\hat{y})\exp(-\mathrm{i}\omega_L t) + \hat{z}$, one finds the Larmor frequency

$$\omega_L = \frac{\mu_B}{\hbar} . \tag{1.6}$$

The Larmor frequency characterizes the precession of μ locally around a field $\mathbf{H}$.

The above considerations apply for multi-electron atoms, however we should at this point take electron spin $\mathbf{S}$ into account. In this case we consider the total angular momentum $\mathbf{J} = \mathbf{L} + \mathbf{S}$, so that there are two contributions to the angular momentum and correspondingly two contributions to the magnetic moment. Denoting these μ_S and μ_L, the total moment is now $\mu = \mu_L + \mu_S$, with magnitude

$$\mu = g\mu_B \sqrt{j(j+1)}\,, \tag{1.7}$$

where j is the angular momentum quantum number. The g-factor is defined by the total, orbital, and spin quantum numbers j, l, and s as

$$g = 1 + \frac{j(j+1)+s(s+1)-l(l+1)}{2j(j+1)}\,. \tag{1.8}$$

The gyromagnetic ratio $\gamma = -g\mu_B/\hbar$ determines the ratio of magnetic moment to angular momentum via $\mu = \hbar\gamma J$. Note that the total moment μ is generally not in the direction of **J**.

1.2.2 Mechanisms for Exchange

In some materials, strong correlations between magnetic moments exist that give rise to long range ordering and thermodynamic phases. The energy associated with these correlations can arise from different mechanisms. The largest of these energies are associated with the Coulomb interaction, and are often referred to as "exchange energies". Before discussing mechanisms for exchange, it is useful to review the relevant energy scales in matter. Following Anderson and Mattis, [1] we summarize some key energy scales in Table 1.1.

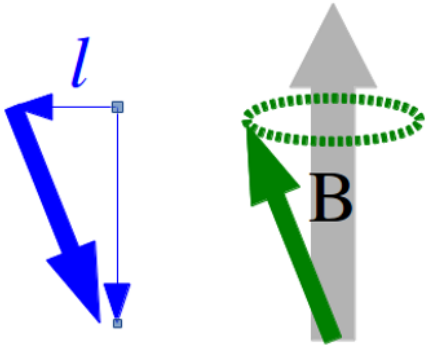

Fig. 1.1 Illustration of precession of an orbital magnetic moment. The angular momentum is oriented opposite to the moment, and the transverse component rotates about axis defined by the local field

Table 1.1 Relevant energy scales for materials, as tabulated by P. W. Anderson

Energy Range (eV)	Mechanisms
$1-10$	Atomic Coulomb integrals; Electronic band widths; Energy/state at ε_F
$0.1-1.0$	Crystal field splitting
$10^{-2}-10^{-1}$	Spin-orbit coupling; $k_B T_C$ or $k_B T_N$
10^{-4}	Magnetic spin-spin coupling; Interaction of a spin with a 1 T field
$10^{-6}-10^{-5}$	Hyperfine electron-nuclear coupling

The Coulombic interaction is the most important for correlating individual magnetic moments, however quantum mechanical effects must be taken into account. In particular, the correlation energy for insulators is determined by overlap of atomic orbitals and these are strongly dependent on the spin state of electrons occupying the orbitals. As we will see, this provides an important insight into the nature of magnetic ordering via exchange.

We can appreciate the strength of the interaction by the following qualitative argument. Pauli exclusion acts to separate electrons in the same spin state. Suppose two electrons are in orbitals on neighbouring atoms. Further suppose that their average separation with antiparallel spins is 0.3 nm, whereas with parallel spins the average separation changes to 0.31 nm. The corresponding change in Coulombic energy is $\Delta E = 0.05$ eV. In units of temperature, this is 580 K. The equivalent field is $\Delta E/\mu_B = 870$ T.

A great insight into how to think about exchange can be obtained by calculating more precisely the exchange energy of overlapping orbitals on neighbouring atoms. A simple model is represented by the following hamiltonian for two nuclear cores (located at positions $\mathbf{R}_a$ and $\mathbf{R}_b$) and two electrons (located at positions $\mathbf{r}_1$ and $\mathbf{r}_2$ defined relative to an atomic core)

Fig. 1.2 Sketch of two orbitals and the average distance for two different spin orderings

$$H = \frac{p_1^2}{2m} + \frac{p_1^2}{2m} + \frac{e^2}{|\mathbf{R}_a - \mathbf{R}_b|} - \frac{e^2}{|\mathbf{r}_1|} - \frac{e^2}{|\mathbf{r}_2|} + \frac{e^2}{|\mathbf{r}_1 - \mathbf{r}_2|} \,. \tag{1.9}$$

The first two terms represent the electron kinetic energies, the third term is the repulsion between cores, the fourth and fifth term is the interaction between the electrons and their respective cores, and the last term is the electron-electron repulsion. The two electron problem can be solved in terms of product orbitals, defined as the two possible orbital occupations of the electrons

$$\Psi_I = \psi_a(\mathbf{r}_1)\psi_b(\mathbf{r}_2) \tag{1.10}$$
$$\Psi_{II} = \psi_a(\mathbf{r}_2)\psi_b(\mathbf{r}_1) \,. \tag{1.11}$$

The two electron wavefunction is a linear combination of these two orbitals

$$\Psi = c_I \Psi_I + c_{II} \Psi_{II} \,. \tag{1.12}$$

Substitution into the hamiltonian of (1.9) allows us to solve for energies and coefficients. Two cases result: a symmetric ($c_I = c_{II}$) and an antisymmetric ($c_I = -c_{II}$) one. The energy of the symmetric case is

$$E_+ = 2E + \frac{V+U}{1+l^2} \,, \tag{1.13}$$

and the antisymmetric case is

$$E_- = 2E + \frac{V-U}{1-l^2} \,. \tag{1.14}$$

The overlap integrals appearing in these energies are

$$V = \int\int \Psi_{I,II}^2 e^2 \left(\frac{e^2}{|\mathbf{R}_a - \mathbf{R}_b|} - \frac{e^2}{|\mathbf{r}_1|} - \frac{e^2}{|\mathbf{r}_2|} + \frac{e^2}{|\mathbf{r}_1 - \mathbf{r}_2|} \right) \mathrm{d}\mathbf{r}_1 \mathrm{d}\mathbf{r}_2 \tag{1.15}$$
$$U = \int\int \Psi_I^* \Psi_{II} e^2 \left(\frac{e^2}{|\mathbf{R}_a - \mathbf{R}_b|} - \frac{e^2}{|\mathbf{r}_1|} - \frac{e^2}{|\mathbf{r}_2|} + \frac{e^2}{|\mathbf{r}_1 - \mathbf{r}_2|} \right) \mathrm{d}\mathbf{r}_1 \mathrm{d}\mathbf{r}_2 \tag{1.16}$$
$$l = \int \psi_a(\mathbf{r})^* \psi_b(\mathbf{r}) \mathrm{d}\mathbf{r} \tag{1.17}$$

The exchange energy J_{ex} corresponds to the difference

$$J_{ex} = E_- - E_+ \sim U l^2 - V \,. \tag{1.18}$$

This is called "exchange" because the symmetric and antisymmetric cases are tied to the requirement of antisymmetric symmetry imposed by Pauli exclusion. The total wavefunction for the two electrons must be antisymmetric. This is accomplished by a product of a symmetric spatial wavefunction with an antisymmetric spin function, or the product of an antisymmetric spatial wavefunction with a symmetric spin function. Note that the antisymmetric spin function has spin zero, whereas the symmetric spin function can have spin $-1, 0$ or 1.

The magnitude of the energy J_{ex} is determined by the Coulomb interaction, and can be indexed to the possible spin states of the two electrons. This feature was noticed independently by Dirac and Heisenberg, who then established that a basis of spin functions could be used to produce the same energy eigenvalues. This allows one to rewrite the hamiltonian in terms of Pauli spin operators: i.e., $H = -J_{ex}\sigma_1 \cdot \sigma_2$. A number of authors, including van Vleck, extended this idea to multi-electron orbitals, producing what is now often called, the exchange hamiltonian

$$H_{ex} = -\sum_{i,j} J_{ex}(\mathbf{r}_i - \mathbf{r}_j)\mathbf{S}(\mathbf{r}_i) \cdot \mathbf{S}(\mathbf{r}_j) \, . \tag{1.19}$$

There are many issues involved with creating a theory for the exchange integral $J_{ex}(\mathbf{r}_i - \mathbf{r}_j)$ for a many atom system. Methods based on perturbation theory have been successful in estimating J_{ex} for many insulating magnets. More details and links to original literature can be found in many standard texts, including [1], [2], and [3]. The problem of constructing an analogous picture for conducting magnets will be discussed later.

We conclude this session by commenting on the sign and range of J_{ex}. The sign can be either positive or negative, depending upon details of the specific overlap integrals. The convention is usually that positive exchange leads to parallel ordering of magnetic moments (ferromagnetism) and negative exchange leads to antiparallel ordering (antiferromagnetism). In many compounds, magnetic ions sit in inequivalent sites with different valences, and can have differently sized magnetic moments. When these order antiferromagnetically, there can still be a residual magnetic moment. These orderings are called ferrimagnetic . Examples are sketched in Fig. 1.3.

In such materials, exchange is mediated by hopping of electrons through orbitals on neighbouring, non-magnetic atoms such as oxygen or fluoride. In these cases additional considerations enter concerning the occupancy and

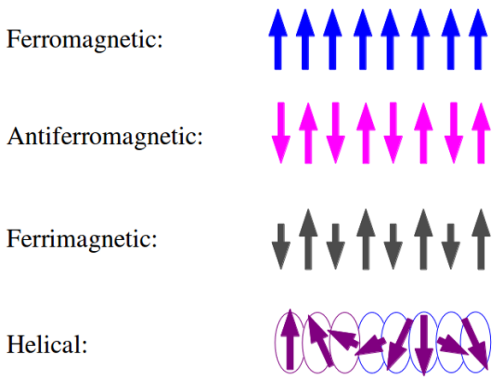

Fig. 1.3 Sketches of four different types of magnetic orderings: parallel (ferromagnetic), antiparallel (antiferromagnetic and ferrimagnetic), and non-colinear (helical in this case)

geometry of multielectron orbitals. The results describe mechanisms for exchange that include what are called "super" and "double" exchange.

Interactions between magnetic atoms beyond nearest neighbour can be signficant. Depending on the geometry, it is possible to have competing ferro- and antiferromagnetic interactions. This can lead to non-colinear orderings, such as the helical ordering depicted in Fig. 1.3. In some cases of particularly low symmetry, it is possible to have interactions that are described by exchange energies of the form $\mathbf{D} \cdot \mathbf{S}_1 \times \mathbf{S}_2$, where $\mathbf{D}$ is a vector that may describe, for example, distortions of the crystal lattice associated with strain fields. This form often appears in descriptions of magnetoelectric effects.

1.3 Response to Applied Magnetic Fields

Experimental studies of magnetic phenomena are quite often made through measurement of response to magnetic fields. There are a number of aspects to this, and we will begin by defining the magnetic susceptibility and how it varies with temperature.

1.3.1 Magnetic Susceptibility

Measurement of macroscopic samples usually involves some sort of averaging over atomic moments. Because of this, it is useful to define a magnetic moment per volume V, called the "magnetization" M

$$\mathbf{M} = \frac{1}{V}\sum_i \mu_i \,. \tag{1.20}$$

The linear response to a magnetic field H is characterized by a susceptibility χ

$$\mathbf{M} = \chi \mathbf{H} \,. \tag{1.21}$$

In general χ is a tensor, but we consider here only the simpler case of an isotropic magnetic system such that the magnetization responds in a direction defined by the orientation of the applied field. This can be along the field direction, or opposite. We consider first the case of non-interacting moments. If the response is in the direction of the magnetic field, it is called "paramagnetic". Example materials include rare earth ions and alkali metals, and typical values range from 10^{-2} to 10^{-4} per mole. If the response is opposite to that of the applied field, the response is called "diamagnetic". Electrons in nearly all materials have some sort of diamagnetic response, and typical values are on the order of -1.0×10^{-6} per mole.

1.3.1.1 Langevin Diamagnetism

The Langevin picture of diamagnetism follows directly from our Bohr orbital model discussed earlier in relation to the Larmor frequency. Using the Larmor frequency $\omega_L = \mu_o He/(2m)$, we can write (following Kittel [4])

$$\mu = I\pi r^2 = \left(-\frac{e\omega_L}{2\pi}\right)\pi r^2 = -\frac{e^2\mu_o H}{4m}r^2 \,. \tag{1.22}$$

We can generalise this to a multi-electron Bohr atom by noting that orbits can occur in any plane, so that the projection of an orbit onto a plane perpendicular to the field $\mathbf{H}$ is on average $2/3$ of the Bohr radius $\sqrt{x^2+y^2+z^2}$. Additionally, the moment scales with the number of contributing electrons Z. The diamagnetic moment then becomes

$$\mu = -\frac{Ze^2\mu_o}{6m}H\langle r^2\rangle \tag{1.23}$$

so that the susceptibility is $\chi_{dia} = -Ze^2\mu_o\langle r^2\rangle/(6m)$. This is negative so that application of an external field induces a moment opposite the field direction.

1.3.1.2 Paramagnetic Suceptibility

Paramagnetism can occur in atoms and molecules with an odd number of electrons so that the total electronic spin is not zero. Defects in crystals can also support such states. Likewise, free atoms and ions with partly filled inner shells can support uncompensated spin. Examples include Mn^{2+} and Gd^{3+} . In some cases solids constructed from such ions will be paramagnetic. We will also see that paramagnetism can appear over restricted temperature ranges in some materials. Finally, we will later mention superparamagnetism where nanoscopic dimensions lead to paramagnetic behaviour.

One obvious example of this is hydrogen. Hydrogen atoms have spin $1/2$ and no orbital moment in the ground state. In this case $J = S$ and $E = -\mu_o\mu H = -\mu_o\mu_B H$ since $g \approx 2$ and $S = 1/2$. Writing $B = \mu_B|H|$, the energy is $E = \mp\mu_B B$, where the minus sign applies when the moment is parallel to H, and the plus sign applies when the moment is antiparallel to H.

We next consider what happens at finite temperatures. When $B = 0$, the number of up spins and down spins should be equal since "up" and "down" are arbitrary. This should also be true at high temperatures even with non-zero field if $k_BT \gg |E|$. However at low temperatures with finite field, one expects more spin up than spin down since the up state is energetically favored. As a function of field, we expect that at low temperatures the populations of up spins will saturate as the field strength is increased, and the population of down spins will tend to zero.

We can make these considerations precise by calculating the fractions of up and down spins according to Boltzman statistics. The fraction $N_\uparrow$ of N spins should be proportional to the thermal probability to be in the $E < 0$ state

$$\frac{N_\uparrow}{N} = \frac{1}{Z}\mathrm{e}^{+\frac{\mu_B}{k_BT}} , \tag{1.24}$$

where Z is a constant for normalization. The fraction of down spins, $N_\downarrow$, should go as

$$\frac{N_\downarrow}{N} = \frac{1}{Z} e^{-\frac{\mu_B}{k_B T}} . \tag{1.25}$$

Normalization gives Z as

$$Z = e^{\frac{\mu_B}{k_B T}} + e^{-\frac{\mu_B}{k_B T}} . \tag{1.26}$$

The difference in populations is the average magnetic moment

$$\langle \mu \rangle = \mu_B N \tanh\left(\frac{\mu_B B}{k_B T}\right) . \tag{1.27}$$

For $B = 0$, this gives zero moment at any temperature, as expected. For large T, the lowest order term is linear in B and one has

$$\langle \mu \rangle = \mu_B N \frac{\mu_B B}{k_B T} \tag{1.28}$$

so that the susceptibility is

$$\chi_{para} = \frac{\langle \mu \rangle}{B} = \frac{\mu_B^2 N}{k_B T} . \tag{1.29}$$

The inverse dependence on temperature is the Curie Law: $\chi_{para} = C/T$ where C is the Curie constant. This is a useful experimental parameter to measure, and the inverse is usually plotted as a function of temperature, allowing the Curie constant to be determined from the slope.

The above equations for χ_{para} are valid for spin $1/2$. Generalisation to arbitrary angular momentum J is straightforward. A higher value of J corresponds to more possible angular momentum states, and the thermal average needs to account for these different possible values. The average moment is then defined as

$$\langle \mu \rangle = \frac{1}{Z_J} \left(\sum_j e^{\mu_B j B} - \sum_j e^{-\mu_B j B} \right) . \tag{1.30}$$

The sum and normalization factor can be worked out, and the result is

$$\langle \mu \rangle = N g J \mu_B B_J \left(\frac{g J \mu_B}{k_B T}\right) , \tag{1.31}$$

where $B_J(x)$ is the Brillouin function, and defined by

$$B_J(x) = \frac{2J+1}{2J}\coth\left(\frac{2J+1}{2J}x\right) - \frac{1}{2J}\coth\left(\frac{x}{2J}\right) . \tag{1.32}$$

The first term in an expansion of 1.32 for small x is linear in $1/T$, consistent with the Curie Law. It is useful to note that values of C will depend very much upon the relative contributions of the spin and orbital components of the magnetic moment. In materials this will involve details of how the spin and orbital angular momenta couple. An extended tutorial discussion can be found in [5].

1.3.1.3 Paramagnetism of Metals

Experimentally, metals show a weak paramagnetic response. This is not what one expects from classical arguments such as those discussed in the previous section. Instead for metals one finds that the paramagnetic susceptibility is roughly independent of temperature. This turns out to be another consequence of Pauli excusion and spin, and can be understood as follows.

The important electron states in a metal are those near the Fermi energy ε_F . In terms of the number, or density, of states at energy ε one can expect a density of states $D(\varepsilon)$ to be roughly of the form shown in Fig. 1.4. The left panel shows the spin up and down density of states without an applied field, and the panel on the right shows the state densities with an applied field. A non-zero applied field favours magnetic moments that are parallel to the field direction, and so lowers the electronic energies of the spin down electrons. Likewise, the electronic energies of up spin electrons is increased.

The shift in energy per spin is $\pm\mu_B B$, leading to an imbalance of numbers between spin up and spin down states that lie beneath the Fermi energy. This corresponds to an overall magnetic moment that is approximately given by

$$\langle\mu\rangle = \frac{1}{2}g\mu_B\left(D(\varepsilon_F)\mu_B B\right) , \tag{1.33}$$

where the factor $1/2$ appears since $D = D_\uparrow + D_\downarrow$. Using results for free electron gases, $D(\varepsilon_F) = 3N/(2k_B T_F)$, where $k_B T_F = \varepsilon_F$. One then arrives at

$$\chi_P = \frac{2N\mu_B^2}{2k_B T_F} , \tag{1.34}$$

independent of temperature. Note that at room temperatures, $\chi_{para}/\chi_P \ll 1$ so that contributions to metallic paramagnetism are due almost exclusively to field induced shifts of the electronic energies. We note that the diamagnetic contribution is significant: Landau showed that it is given by $\chi_{dia} = -\chi_P/3$.

1.3.1.4 Magnetic Ordering in Correlated Spin Systems

We now consider the case when interactions between spins represented by exchange energies lead to long range ordering. Following on from our discussion of paramagnetic response in the previous sections, one can imagine that at finite temperatures the thermal reduction of magnetization arises due to local misalignments of magnetic moments with a local field.

Consider a ferromagnet in which the ground state is one with parallel spins. In the sketch shown in Fig. 1.5, a "snapshot" of spins randomly deviated away from parallel alignment is shown. If one considers a single spin, as indicated by the circle, on average the local exchange field will be proportional to the thermally averaged spin of the system. This is as if the local exchange field were being produced by static, aligned, neighbouring spins with reduced magnitudes. This interaction is depicted on the right hand side by purple coloured arrows surrounding a fluctuating spin.

This approximation to the local field is an example of mean field theory, and is represented by writing

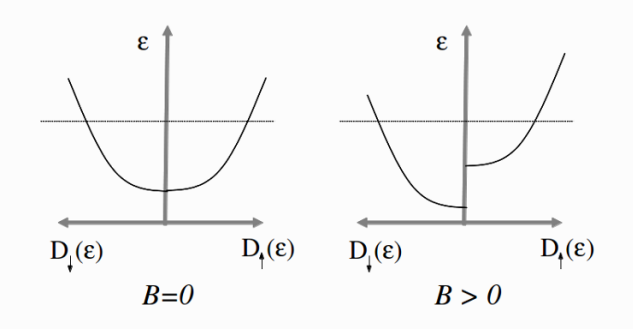

Fig. 1.4 Sketch of density of states for a nonmagnetic metal as a function of energy. In zero applied field the state distributions are independent of spin. An applied field breaks the symmetry of the up and down states

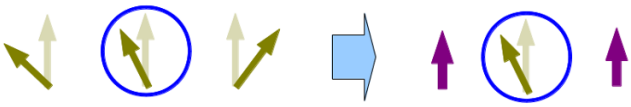

Fig. 1.5 The mean field approximation amounts to replacing the local field of a moment (indicted here by a circle) with a field proportional to the average magnetization of the entire system (represented by purple arrows)

$$\mathbf{B}_{ex} = \lambda \mathbf{M} = \left(\frac{2Z_{nn}J_{ex}}{N\mu_B} \right) \mathbf{M} \,, \tag{1.35}$$

where $\mathbf{M}$ is the magnetization and λ is a constant representing the exchange integral and the number of nearest neighbours Z_{nn} . The field B_{ex} is sometimes called a Weiss molecular field. At zero temperatures this is entirely equivalent to the classical form of the Heisenberg hamiltonian.

At finite temperatures, this approach provides a good first approximation to thermal reduction of magnetic order. In this picture, B_{ex} adds to the external applied field, and one can define a susceptibility based on that for χ_{para}

$$\chi = \frac{C}{T - \lambda M} \,. \tag{1.36}$$

Solving for M/B , one arrives at

$$\chi_F = \frac{C}{T - T_C} \,, \tag{1.37}$$

where $T_C = \lambda C$. This susceptibility shows that a ferromagnetically ordered system can behave as a paramagnet above some critical temperature T_C . Below this temperature, ordering due to exchange will dominate, and (1.37) will not apply. Above T_C, $1/\chi_F$ is linear in temperature, but intersects the temperature axis at T_C, a clear experimental signature of the possibility of an onset of magnetic ordering.

Below T_C, we need to revist the calculation of thermal averages. In zero applied field, there is still a non-zero probability of finding an average magnetization at finite temperatures. Consider a simplified model in wich magnetic moments μ only point up or down with respect to one another (corresponding to the spin half case above). Denoting the numbers pointing up with N_+ and those down with N_- , the fractions are

$$\frac{N_{\pm}}{N} = \frac{e^{\pm\frac{\mu\lambda M}{k_B T}}}{e^{\frac{\mu\lambda M}{k_B T}} + e^{-\frac{\mu\lambda M}{k_B T}}} . \tag{1.38}$$

The difference between up and down fractions again gives the magnetization. This is

$$M = \mu_B N \tanh\left(\frac{\mu\lambda M}{k_B T}\right) . \tag{1.39}$$

This is an implicit equation for M , and can be solved graphically when put in the form $x = \tanh(x)$. A solution for $M = 0$ always exists, but an additional solution for $M > 0$ exists for temperatures between $T = 0$ and $T = T_{mf}$, where T_{mf} is the critical temperature corresponding to T_C in the Curie theory.

The theory can be generalised to larger J values as before, with the result that self consistent equation now has the form

$$M = Ng\mu_B J B_J\left(\frac{g\mu_B\lambda M}{k_B T}\right) . \tag{1.40}$$

Solutions for M for different values of J are shown in Fig. 1.6. Note that the critical temperature is determined by J_{ex}, not the angular momentum number J.

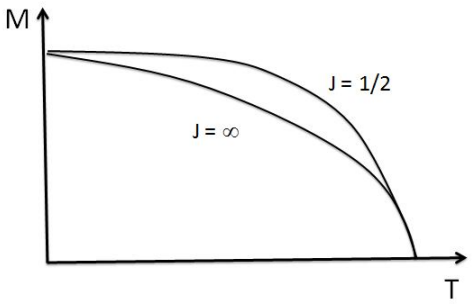

Fig. 1.6 Solution of (1.40) for different values of angular momentum quantum number J

We note that this mean field description of temperature dependence is a strong approximation, and breaks down in a number of ways. The problem is

that it neglects correlations which are important at low temperatures and also near T_C. Moreover, it is also not able to capture effects associated with dimensionality. These aspects will be discussed later when we introduce models for fluctuations.

We complete this section with a few words about antiferromagnetic ordering. The simplest example of antiferromagnetic ordering is to reverse the direction of neighbouring moments, as depicted earlier in Fig. 1.3. This can be modelled simply by changing the sign of J_{ex}, or equivalently, the sign of λ . One can again show that a paramagnetic response exists above a critical temperature T_N, but the susceptibility is now

$$\chi_{AF} = \frac{C}{T + T_N} \,. \tag{1.41}$$

In this case the inverse susceptibility is still linear in T, but it now intercepts the temperature axis at a negative value. The three susceptibilities discussed above are plotted in Fig. 1.7 for comparison.

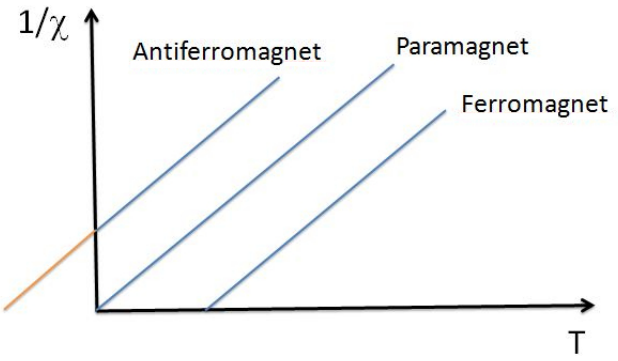

Fig. 1.7 Examples of paramagnetic susceptibilities. A simple paramagnet is compared with a ferromagnet (with $T > T_C$) and an antiferromagnet (with $T > T_N$)

1.3.2 Magnetic Ordering and Magnetoelectric Coupling

As noted earlier, non-collinear ordering of spins can arise from competing exchange interactions in some classes of materials. The Dzyaloshinski-Moriya interaction is often used to provide a phenomenological description of interactions that lead to a so-called "weak" ferromagnetism arising from canted moments in an otherwise antiferromagnetic ordering.

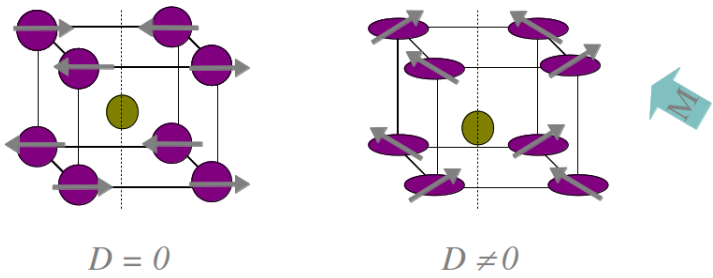

Fig. 1.8 The spin structure in a material such as $BiFeO_3$ would be antiferroelectric for a crystal with inversion symmetry, such as that depicted on the left. A Dzyaloshinski-Moriya interaction can arise for distortions that remove inversion symmetry, leading also to a canting of spins as shown on the right

An example is shown in Fig. 1.8, where spins in a cubic lattice align antiparallel if D is zero in a hamiltonian of the form $H = \sum_{i,j}[J\mathbf{S}_i \cdot \mathbf{S}_j - D\mathbf{S}_i \times \mathbf{S}_j]$.

In some multiferroic materials, a coupling between dielectric and magnetic order parameters exists. One model for this is through a Dzyaloshinski-Moriya interaction with a coupling constant that depends on the dielectric polarization P . A geometry for this is shown in Fig. 1.9. A phenomenological free energy for such a system can be written as

$$F = \frac{1}{2}\beta_1 P^2 + \frac{1}{4}\beta_2 P^4 - PE - \lambda \mathbf{m}_a \cdot \mathbf{m}_b - K(m_a^2 z + m_b^2 z) - MH + F_{ME} \ . \quad (1.42)$$

The first three terms in (1.42) are a continuous transition Landau-Ginzburg energy density for the ferroelectric component, with landau parameters β_1 and β_2. The third term is the energy of a static electric field applied along the

direction of P. The next three terms are the exchange, anisotropy (assumed to be uniaxial along the z direction) and the Zeeman field aligned along the canting direction. The final term is the magneto-electric coupling, which is often taken as a Dzyaloshinski-Moriya form. An example appropriate for $BaMnF_4$ and $FeTiO_3$ is [6]

$$F_{ME} = -\alpha P(\mathbf{m}_a + \mathbf{m}_b)_x(\mathbf{m}_a - \mathbf{m}_b)_z = -\alpha P M_x L_z \,. \tag{1.43}$$

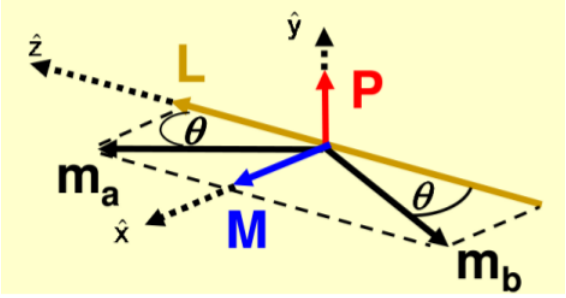

Fig. 1.9 Weak magnetization for a canted antiferromagnet in a multiferroic. Here there are two sublattices with magnetizations $\mathbf{m}_a$ and $\mathbf{m}_b$. **L** and **M** are the sum and differences between the sublattice magnetization vectors. A dielectric polarization **P** is oriented perpendicular to the plane of canting. **L** and **M** are the sum and differences between the sublattice magnetization vectors

The temperature dependence of the magnetization can be calculated in a mean field approximation as described earlier. The temperature dependence of the ferroelectric is obtained from the Landau-Ginzburg parameter $\beta_1 \sim (T - T_f)$ where T_f is the critical temperature of the ferroelectric. The canting angle determining M is found by minimizing the total free energy with respect to the orientations of the magnetic sublattices and the magnitude of P . An example is shown in Fig. 1.10 where parameters are chosen to represent $BaMnF_4$. Results for different strengths of magnetoelectric coupling are shown.

For this material, the ordering temperature T_f for the ferroelectric is larger than that for the magnetic ordering. The magneto-electric coupling serves to enhance the dielectric polarization at low temperatures when M is non-zero, but the enhancement disappears when M goes to zero. Also, the magnetoelectric energy favours orientation of M and P such that M will reverse if P is

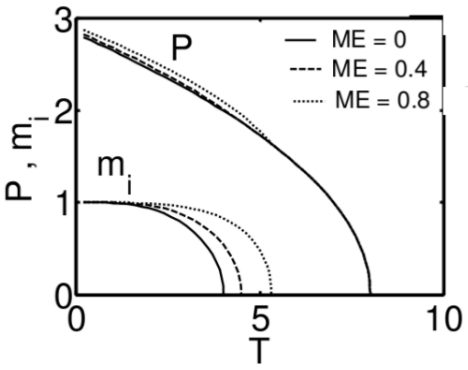

Fig. 1.10 Temperature dependence of a the ferroelectric and magnetic components calculated for a model multiferroic. After [6] (Used with permission)

reversed, or P will reverse if M is reversed. Thus one can control the orientation of P with a magnetic field, and the orientation of M with an electric field.

1.3.3 Magnetic Impurities in Metals

We mention briefly another type of magnetic ordering interaction that is mediated by conduction electrons. Consider a local magnetic moment immersed in a nonmagnetic metal. Spin dependent scattering of conduction electrons from the impurity will result in oscillations of the spin density in proximity to the impurity, in analogy to Friedel oscillations. The period of oscillations depends upon the Fermi wavevector of the conduction spins.

A second magnetic impurity placed some distance r away from the first will likewise interact with the conduction spins. The electronic states responsible for the magnetic moment of the impurity will hybridize to some extent with the conduction band of the host metal. As a result, the relative orientation of the impurity moments will have an energy associated with the oscillations in the conduction spin densities. The energy will depend on the separation r of the impurities, and favour parallel alignment of the moments for some dis-

tances, and antiparallel alignment for other distances. The lowest order terms for this energy are

$$F(r) = \frac{\sin(2k_F r) - 2k_F r \cos(2k_F r)}{(2k_F r)^4} , \tag{1.44}$$

where k_F is the magnitude of the fermi wavevector. This interaction is responsible for the oscillatory magnetic coupling between ferromagnets across thin transition metal films and known as the Ruderman-Kittel-Kasuya-Yosida interaction [7]. In an alloy such as CoMn or AuMn, where local moments are distributed randomly, this interaction can give rise to frustration due to competition between parallel and antiparallel ordering energies.

1.3.4 Magnetic Metals

It is possible to find some metals with spins that order spontaneously without the application of an external magnetic field. Consider transition metals which have a both *s* and *d* like states at the Fermi energy. The energy states for a non-magnetic metal are degenerate with respect to the spin state of the electrons.

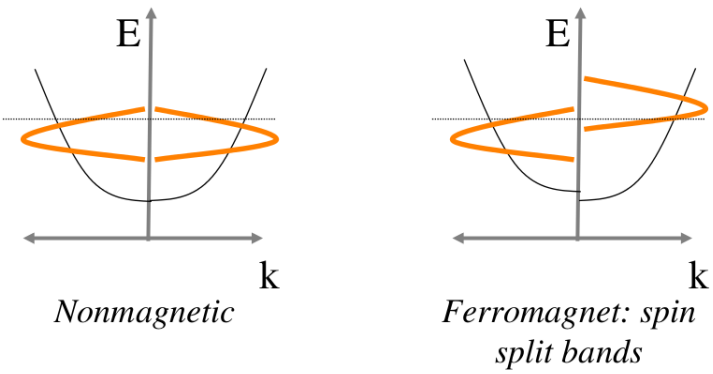

Fig. 1.11 Left: Sketch of energies for *s* and *d* bands of a non-magnetic transition metal. Right: Some metals have spontaneous splitting of spin up and down levels, creating a net magnetization

A sketch of this is shown in Fig. 1.11. The d band is narrow compared to the s band, and is found in some metals to have spin dependence for sufficiently low temperatures. In these cases, there is a majority of spins of one orientation, and the material has a ferromagnetic magnetization.

A simple way to conceptualise this is with the single band Stoner model. The central idea is that Pauli exclusion creates correlations between spins, which was also the principle underlying the theory for the exchange integral for insulators. In the case of conductors, we can think of a Hubbard hamiltonian with a correlation energy U of the form

$$Un_{\downarrow\uparrow} = \frac{1}{4}U[n^2 - (n_\uparrow - n_\downarrow)^2] \,, \tag{1.45}$$

where $n_\uparrow$ and $n_\downarrow$ are the number of up and down spins in the band, and $n = n_\uparrow + n_\downarrow$. The magnetization is then defined as $M = n_\uparrow - n_\downarrow$. The Stoner model then proposes a spin dependent potential for single electron energies where the spin up/down energies are given by

$$\varepsilon_{\uparrow\downarrow}(k) = \varepsilon_o(k) - \frac{I}{n}n_{\uparrow\downarrow} \,. \tag{1.46}$$

Here $\varepsilon_o(k)$ is the non-magnetic energy level, and I is the so-called Stoner parameter, which relates to the correlation energy.

One can now calculate a susceptibility to an applied magnetic field. This can be approached by calculating $\langle M(k)\rangle$ using a free energy hamiltonian, and then requiring $\partial\langle M(k)\rangle/\partial t = 0$. This can be used to derive a relation between M and the applied field B, from which the susceptibility is identified. One finds an enhanced Pauli susceptibility (χ_P)

$$\chi = \frac{\chi_P}{1 - ID(\varepsilon_F)} \,. \tag{1.47}$$

The key result is that the unpolarized ground state becomes unstable when $D(\varepsilon_F)I = 1$. A magnetically ordered ground state can appear then for a sufficiently large density of states at the Fermi level. It is useful to note that there exist metals which have an enhancement factor that is not large enough to provide spontaneous order, but can result in the appearance of local moments induced by magnetic impurities immersed in a paramagnetic host. This has been observed for impurities in Pd and interfaces of Pt with ferromagnetic metals.

1.4 Magnons and Thermal Fluctuations

It was noted at the end of the last section that mean field theory breaks down when correlations between spins become important. We can see how mean field theory neglects fluctuations by looking at how the mean field approximation is applied to the Heisenberg hamiltonian. Assume a hamiltonian for classical spins of the form

$$H = -\frac{1}{2}\sum_{<i,j>} J_{ex}\mathbf{S}_i \cdot \mathbf{S}_j \,, \tag{1.48}$$

where the notation $< i, j >$ is used to indicate that the sum is over only near neighbours. The factor of $1/2$ appears because spin pairs are counted twice. The minus sign ensures that a positive exchange integral J_{ij} leads to ferromagnetic ordering. Now consider fluctuations $\mathbf{s}_i$ at site i defined relative to the mean $\langle S \rangle$. These are written as

$$\mathbf{S}_i = \mathbf{s}_i + \langle S \rangle \,. \tag{1.49}$$

Substitution into the hamiltonian of (1.48) produces the expression

$$H = -\sum_{i,\delta} J_{ex}\mathbf{s}_i \cdot \mathbf{s}_\delta + Z_{nn}N\,|\langle \mathbf{S} \rangle|^2 - 2\sum_i Z_{nn}J_{ex}\mathbf{S}_i \cdot \langle \mathbf{S} \rangle \,. \tag{1.50}$$

The first term represents contributions from interactions between fluctuations, and the last term is the interaction of the fluctuations with the mean magnetization. The mean field approximation amounts to neglecting the first term.

Interactions between fluctuations create correlations that can become important in determining the thermal behaviour of the spin system. At high temperatures near the critical point, correlations can occur over any lengthscale. Mean field theory predicts that at these temperatures $\langle \mathbf{S} \rangle \sim (T - T_C)^{1/2}$. When correlations are taken into account, $\langle \mathbf{S} \rangle \sim (T - T_C)^{\beta}$, where $\beta \approx 0.34$ for ferromagnets. Moreover, dimensionality is very important: It is expected in two dimensions for any finite temperature that there is no long range ordering if the interactions are only through short range exchange.

1.4.1 Magnons in Insulators

At low temperatures, $\langle \mathbf{S} \rangle$ is not much changed from its zero temperature value in a mean field model, and deviations from the mean field behaviour are directly attributable to the correlations described by the first term in (1.50). The nature of these low temperature excitations can be understood through an insight provided by Holstein and Primakoff. They noticed that the angular momentum ladder operators $L_{\pm}$, defined to act on an angular momentum function $\psi_{m,l}$ according to

$$L_{\pm}\psi_{m,l} = \hbar\sqrt{(l \mp m)(l \pm m + 1)}\,\psi_{m\pm 1,l} \,, \tag{1.51}$$

can be put in the form of harmonic oscillator raising and lowering operators. The idea is to define a spin deviation number n_s from the angular momentum quantization numbers l and m according to $n_s = l - m$. n_s can be thought of as the number of quanta associated with a reduction of L_z from its minimal value.

The correspondence to harmonic oscillators is made in the limit of small n_s. In this case, the raising and lowering operators become

$$L_{+}\psi_{n_s} \approx \hbar\sqrt{2l}\sqrt{n_s}\,\psi_{n_s-1} \tag{1.52}$$

$$L_{-}\psi_{n_s} \approx \hbar\sqrt{2l}\sqrt{n_s+1}\,\psi_{n_s+1} \,. \tag{1.53}$$

These have exactly the same form as harmonic oscillator raising and lowering operators. Note that the increase in n_s corresponds to the angular momentum lowering operator. It is therefore convenient to define spin ladder operators in analogy to the harmonic oscillator operators ($a^{+} = x + \mathrm{i}p_x$, for example) as

$$S^{-}\psi_{n_s} = \sqrt{2S}\sqrt{2S}a^{+}\psi_{n_s} = \sqrt{2S}\sqrt{n_s}\,\psi_{n_s-1} \tag{1.54}$$

$$S^{+}\psi_{n_s} = \sqrt{2S}\sqrt{2S}a\psi_{n_s} = \sqrt{2S}\sqrt{n_s+1}\,\psi_{n_s+1} \tag{1.55}$$

$$S^{z}\psi_{n_s} = (-S + a^{+}a)\psi_{n_s} = (-S + n_s)\,\psi_{n_s} \,. \tag{1.56}$$

The number operator then appears in the definition for S^z, and counts the number of spin excitations. The spin hamiltonian can be expanded in terms of a Fourier expansion of the spin operators, where the operators b_k^{+} and b_k now describe raising and lowering operators for momentum states k

$$S_j^- = \frac{1}{\sqrt{N}} \sum_k \mathrm{e}^{-\mathrm{i}\mathbf{k}\cdot\mathbf{x}_j} b_k \tag{1.57}$$

$$S_j^+ = \frac{1}{\sqrt{N}} \sum_k \mathrm{e}^{\mathrm{i}\mathbf{k}\cdot\mathbf{x}_j} b_k^+ \,. \tag{1.58}$$

The hamiltonian expressed in terms of these operators is now diagonal in low orders of b

$$H = -J_{ex} N z S^2 + \sum_k \left[2 J_{ex} z S \left(1 - \frac{1}{z} \sum_\delta \mathrm{e}^{\mathrm{i}\mathbf{k}\cdot\delta} \right) \right] b_k^+ b_k + \mathscr{O}(b^4) \,. \tag{1.59}$$

The z refers to the number of nearest neighbours. The second term in (1.59) is the magnon contribution to the energy, and the b are magnon operators. For a cubic lattice of constant a, the energy in the long wavelength limit for a ferromagnet is

$$\hbar\omega_k = (J_{ex} S a^2) k^2 \,. \tag{1.60}$$

One can use this approximation to estimate the total reduction of magnetization due to thermal fluctuations. The excitations are bosons, so that the thermodynamic average over fluctuations is estimated using a Bose-Einstein statistics

$$\sum_k \langle b_k^+ b_k \rangle = \frac{1}{(2\pi)^2} \int \left[\mathrm{e}^{\frac{\omega_k}{k_B T}} - 1 \right]^{-1} d^3\mathbf{k} \sim T^{3/2} \,. \tag{1.61}$$

This is the Bloch law describing the reduction of magnetization as a function of temperature. It applies for low temperatures only, and Dyson showed how taking higher order magnon interactions into account, one can expect corrections that go as higher powers of $T^{1/2}$, i.e. $M(0) - M(T) \sim c_1 T^{3/2} + c_2 T^{5/2} + c_3 T^{7/2} + \ldots$ [8].

There are different experimental probes of spinwave excitations, including inelastic neutron scattering, inelastic light scattering, and various microwave absorption techniques. Inelastic neutron scattering is able to sample a wide range of energies across the magnon band structure whereas other techniques typically sample long wavelength excitations near the magnon Brillouin zone center. More will be said in the next sections about long wavelength excitations.

1.4.2 Magnons in Metals

As discussed earlier, one must take electronic band structure into account for a description of metallic magnetism. One can cast this theory in a form reminiscent of the above theory for magnons in insulators by writing the electronic hamiltonian in terms of the fermion analogy to raising and lowering operators. In this picture, we define state and site occupation operators c and c^+whose mathematical effect is to lower or raise the occupation of an electronic state. The hamiltonian in this picture has the form

$$H = \sum_{lm\sigma} H_o c^+_{m\sigma} c_{l\sigma} + \sum_{lm\sigma} \sum_{l'm'\sigma'} H_i c^+_{m\sigma} c^+_{l\sigma} c_{m'\sigma'} c_{l'\sigma'} \ , \tag{1.62}$$

where the energies are the kinetic and positive core interactions (H_o) and the Coulombic repulsion (H_i). The sums are over sites and spin states. These are given by integrals involving the single particle wavefunctions $\psi_j(r)$ associated with site j

$$H_o = \int \psi^*_l(\mathbf{r}) \left[\frac{p^2}{2m} + \sum_{\mathbf{R}} V(\mathbf{r}-\mathbf{R}) \right] \psi_m(\mathbf{r}) \mathrm{d}^3\mathbf{r} \tag{1.63}$$

$$H_i = \int \psi^*_l(\mathbf{r}) \psi^*_{l'}(\mathbf{r}') \frac{e^2}{|\mathbf{r}-\mathbf{r}'|} \psi_{m'}(\mathbf{r}') \psi_m(\mathbf{r}) \mathrm{d}^3\mathbf{r} \ . \tag{1.64}$$

We next define spin raising and lowering operators at site m as

$$S^z_m = \frac{1}{2} \left(c^+_{m\uparrow} c_{m\uparrow} - c^+_{m\downarrow} c_{m\downarrow} \right) \tag{1.65}$$

$$S^+_m = c^+_{m\uparrow} c_{m\downarrow} \tag{1.66}$$

$$S^+_m = c^+_{m\downarrow} c_{m\uparrow} \ . \tag{1.67}$$

This theoretical formulation can be used to identify low energy excitations of the electron gas in a perturbative approach. In the context of a Stoner model wherein the Coulomb interaction is replaced by a local energy $I\delta(\mathbf{r}_i - \mathbf{r}_j)$, the excitation energies are found to obey $\omega_k \ Dk^2$, similar in form to the dispersion for magnons in an insulator. The exchange constant for metals however depends upon details of the band structure and spin densities. Moreover, the magnons run into a band of spin flip excitations (Stoner excitations) for large

wavevectors, that are not found in the Heisenberg model discussed for insulators.

1.5 Macroscopic Models of Magnetic Ordering and Excitations

So far in our treatment we have concentrated on exploring how magnetism arises from underlying electronic states. A more phenomenological description is possible, and preferrable in some cases for understanding and modelling details of many types of experiments. These models start from a continuum formulation of the energies and equations of motion. Comprehensive accounts of original spin wave theories can be found in [9], [2], and [10]. More recent summaries are contained in [12], [11], and [13].

A magnetic density field can be defined in terms of local electronic spins formally as

$$\hat{\mathbf{M}}(\mathbf{r}) = g\mu_B \sum_j \delta(\mathbf{r} - \mathbf{r}_j)\hat{\sigma}_j \; . \tag{1.68}$$

It is most convenient to work with a macroscopic magnetization, $\mathbf{m}(\mathbf{r}) = \mathrm{Tr}(\rho\hat{\mathbf{M}}(\mathbf{r}))$, where ρ is the density matrix. This defines a classical quantity M for the magnetic moment density at a location $\mathbf{r}$ in a material.

1.5.1 Exchange and Anisotropy Effective Fields

An exchange energy can now be postulated that is compatible with the symmetry of the crystal

$$E_{ex} = \sum_{\alpha kl} C_{kl} \frac{\partial m_\alpha(\mathbf{r})}{\partial r_k} \frac{\partial m_\alpha(\mathbf{r})}{\partial r_l} \; , \tag{1.69}$$

where α indexes the components of the magnetization, and k indexes the components of the position vector. In an isotropic medium this becomes, for example,

$$E_{ex} = C\left[(\nabla m_x)^2 + (\nabla m_y)^2 + (\nabla m_z)^2\right] \; . \tag{1.70}$$

There are additional effects associated with the local atomic environment that can also be constructed using symmetry arguments. Small perturbations due to spin orbit coupling can introduce an orientational dependence to the magnetization. Symmetry allowed terms to an expansion of the energy associated with these perturbations can take the form

$$E_{anis} = -K_u m_z^2 + K_4 \left(m_x^2 m_y^2 + m_x^2 m_z^2 + m_y^2 m_z^2 \right) + \ldots , \tag{1.71}$$

where the coefficients K_u and K_4 denote uniaxial and four-fold anisotropies, respectively. As an example, consider hexagonal Co. This crystal has a two fold axis of rotation, and allows uniaxial anisotropies. The two largest terms can be written in terms of an angle θ measured from the axis of rotation

$$E_{ani} = K_u^{(1)} \sin^2 \theta + K_u^{(2)} sin^4 \theta \, . \tag{1.72}$$

A typical value for $K^{(1)}$ is 5×10^5 J/m^3 .

1.5.2 Magnetostatic Fields

Exchange and anisotropy are "local" in the sense that the range of interactions are mostly limited to the immediate atomic environment. Magnetic moments themselves act as sources of magnetic fields through interactions mediated by the electromagnetic field. An individual point moment generates a dipolar magnetic field, and the site local field in an ensemble of point dipoles can be represented by a sum over other dipoles in the system

$$\mathbf{h}_{dip} = \frac{1}{2} g^2 \mu_B^2 \sum_{ij} \left[\frac{\mathbf{S}_i \cdot \mathbf{S}_j}{r_{ij}^3} - 3 \frac{(\mathbf{r}_{ij} \cdot \mathbf{S}_i)(\mathbf{r}_{ij} \cdot \mathbf{S}_j)}{r_{ij}^5} \right] , \tag{1.73}$$

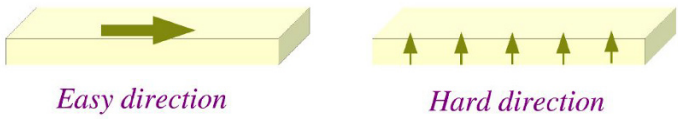

Fig. 1.12 Easy and hard directions sketched for a single domain rectangular magnetic element

where $\mathbf{r}_{ij}$ is the position vector defined by the sites i and j . This interaction is long ranged, and can drive complex magnetic configurations because of dipolar fields created by sources over large lengthscales. The shape of a magnetic element is important in this regards. A uniformly magnetized element will generate demagnetizing fields through the magnetostatic fields that can appear as a "shape anisotropy".

Dipoles with a component normal to a surface generate uncompensated poles. The magnitude of the field produced by surfaces is proportional to the magnetic field flux generated by these poles. In a rectangular planar element, such as that depicted in Fig. 1.12, alignment of the magnetization along the long axis will produce the smallest magnetic field flux, thus defining an "easy" direction for the orientation of the magnetization. Alignment of the magnetization normal to the largest area will generate a correspondingly large flux, and defines a "hard" axis orientation for the magnetization.

It is possible to calculate exactly the demagnetizing fields and energies only for a few simple geometries. A uniformly magnetized ellipsoid will have a shape anisotropy energy density arising from demagnetizing fields, that can be described in terms of shape factors N_x , N_y , and N_z :

$$E_{shape} = \frac{M_S^2}{2\mu_o}(N_x \sin^2\theta\cos^2\phi + N_y \sin^2\theta\sin^2\phi + N_z\cos^2\theta)\,. \qquad (1.74)$$

Calculation of magnetostatic fields for specific element shapes and different magnetic configurations is far from trivial. Although there are some specific geometries which can be treated analytically, in general numerical methods are used. These approaches are called "micromagnetic", and involve various approaches to taking the long range magnetostatic fields into account in addition to local exchange, anisotropy, and other energies.

1.5.3 Spinwaves in Continuum Models

The macroscopic model outlined above can be used to also describe magnonic excitations in the long wavelength limit. We refer to this description as "spinwaves", with the understanding that it is the classical analogue of the quantum physics picture presented earlier.

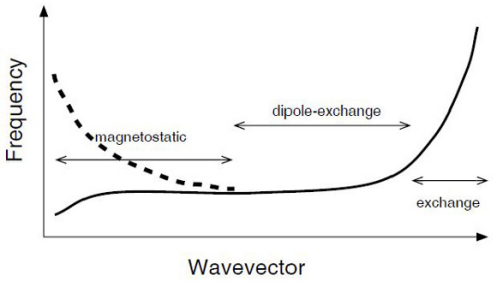

Fig. 1.13 Illustration of different wavenumber regimes for magnetostatic, dipole-exchange, and exchange spin-waves. Propagation directions along the magnetization axis can have negative group velocities at long wavelengths

We begin with a total energy constructed from the exchange, anisotropy, magnetostatic, and any additional contributions that might arise (such as interlayer magnetic coupling, Dzyaloshinski-Moriya interactions, etc). An effective field $\mathbf{H}_{eff}$ can be constructed as a gradient of the energy E_{tot}

$$\mathbf{H}_{eff} = -\nabla_{\mathbf{M}} E_{tot} \ . \tag{1.75}$$

An effective field constructed from an applied field H_a, exchange with strength A, anisotropy with strength K, and a dipolar field $\mathbf{h}_{dip}$ will have the form

$$\mathbf{H}_{eff} = \mathbf{H}_a + A\nabla^2\mathbf{M}(\mathbf{r}) + \mathbf{M}(\mathbf{r}) \cdot K\mathbf{M}(\mathbf{r}) - \mathbf{h}_{dip} \ . \tag{1.76}$$

The dipolar field can be calculated from Maxwell's equations, and is usually done in the magnetostatic limit where $\nabla \times \mathbf{h}_{dip} = 0$. This is valid for the long wavelength limit in non-conductive materials. In the case of ohmic conductors, this condition needs to be augmented with the associated currents generated by the time varying magnetic field.

The equations of motion in this formulation are of the form of torque equations

$$\frac{\partial}{\partial t}\mathbf{M}(\mathbf{r}) = \gamma\mathbf{M}(\mathbf{r}) \times \mathbf{H}_{eff} - \Gamma_{diss} \ , \tag{1.77}$$

where Γ_{diss} is a torque introduced to describe redistribution and loss of energy from the magnetic system. The redistribution occurs because of interactions between spinwaves and interactions with other degrees of freedom in the system (including elastic, electronic, and electromagnetic). In the original form proposed by Landau and Lifshitz, [14] a damping was chosen such that the

magnitude of the magnetization was conserved. This requirement is served by the construction

$$\Gamma_{diss} = \alpha \mathbf{M}(\mathbf{r}) \times (\mathbf{M}(\mathbf{r}) \times \mathbf{H}_{eff}) \, . \tag{1.78}$$

From the point of view of non-conservative dynamics, the dissipation should be of the form $|\mathrm{d}\mathbf{M}/\mathrm{d}t|^2$. A commonly used form is consistent with this (Rayleigh) dissipation is called "Gilbert damping" [15]. In its more common representation, the equations of motion and damping are written explicitly as

$$(1+\gamma^2\alpha^2 M_S^2)\frac{\partial}{\partial t}\mathbf{M}(\mathbf{r}) = \gamma \mathbf{M}(\mathbf{r}) \times \mathbf{H}_{eff} - \gamma\alpha \mathbf{M}(\mathbf{r}) \times \frac{\partial}{\partial t}\mathbf{M}(\mathbf{r}) \, . \tag{1.79}$$

Illuminating discussions of non-linearities, spinwave interactions, and damping processes observed in microwave resonance experiments can be found in [13], [16], [17], and [18].

The zero wavevector excitations are especially important for a variety of resonance experiments. As an example, consider a ferromagnet illuminated uniformly by a microwave frequency alternating field. Suppose further that the ferromagnet has a uniaxial anisotropy along the y direction, and there is a static applied field along the z direction. The effective field acting on the magnetization is

$$\mathbf{H}_{eff} = \hat{z}H_a + \hat{y}\frac{2K}{M_S^2}M \, . \tag{1.80}$$

Ignore dissipation for simplicity. Substitution into the torque equations gives

$$\frac{\mathrm{d}M_x}{\mathrm{d}t} = -\gamma[H_a M_y - (2K/M_S^2)M_z M_y] \tag{1.81}$$

$$\frac{\mathrm{d}M_y}{\mathrm{d}t} = -\gamma[H_a M_x] \tag{1.82}$$

$$\frac{\mathrm{d}M_z}{\mathrm{d}t} = -\gamma[(2K/M_S^2)M_x M_y] \, . \tag{1.83}$$

These equations are non-linear. However if one considers only small amplitude precessions, then $M_x M_y \approx 0$ and the third equation reduces to a statement that M_z is constant. The small amplitude resonance then corresponds to precession of the magnetization around the z direction, with time varying com-

ponents in the transverse plane. The transverse components oscillated with resonance frequency $\omega = \gamma\sqrt{H_a(H_a - 2K/M_S)}$. The precession is elliptical, and exists only for an applied field large enough to align the magnetization in the hard direction $(H_a > (2K/M_S))$.

Non-zero wavevector excitations are spinwaves. If one considers only the exchange interaction, then the additional contribution to the effective field is $A\nabla^2\mathbf{M}(\mathbf{r})$, and the dispersion of plane waves with wavenumber k is

$$\frac{\omega^2}{\gamma^2} = (H_a + Ak^2)(H_a - 2K/M_S + Ak^2) \, . \tag{1.84}$$

Dipolar interactions can also contribute to the dispersion. In the longest wavelength regime, dipolar contributions dominate and can even lead to waves with negative group velocities (backward travelling waves). For some propagation directions, surface magnetostatic waves can exist as excitations localized to interfaces. At short wavelengths, the exchange contribution dominates, and $\omega \sim k^2$. The waves in the intermediate wavelength range are called "dipole-exchange" modes since the exchange and dipolar contibutions are comparable. These ranges are illustrated in Fig. 1.13.

1.6 Reversal of Magnetization

Fig. 1.14 Analogy between reversal of a single domain particle and a double well potential. Thermal activated reversal can be likened to a chemical rate problem

We have discussed linear dynamics in two contexts: first in terms of linear response to quasi-static applied fields, and next in the context of small amplitude precession and spinwaves. The dynamics of magnetization reversal are now examined, and this goes well beyond linear response in either of the pre-

vious senses. Indeed, magnetic systems have often been used as experimental and theoretical models for different aspects of non-linear dynamics and behaviours far from equilibrium. Some of these will be surveyed here, within the context of magnetization reversal mechanisms.

1.6.1 Reversal of Single Domain Particles

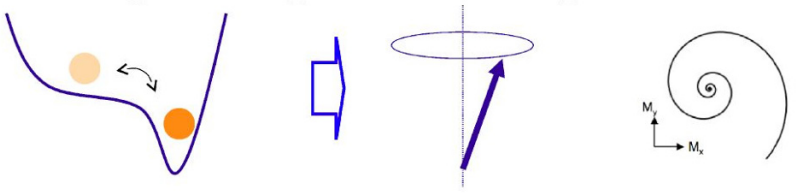

Fig. 1.15 Illustration of the precession driven reversal process. A magnetic field can make an orientation unstable, and reversal then occurs through damped precession

It was noted that the phenomenological equations of motion describing precession are inherently non-linear. A useful conceptual analogy is the double well potential that is perhaps best known from chemical rate theory wherein a barrier separates two minimizing energy states. The barrier must be overcome in order to make the transition from one state to the other.

This analogy is illustrated in Fig. 1.14 where the orientation of a single domain particle is identified with positions in a double well potential. It is assumed that the particle has a large uniaxial anisotropy so that only two alignments parallel with the anisotropy axis are energetically favorable. In magnetic systems, an external magnetic field will break the degeneracy of the two otherwise equivalent configurations, as indicated by the lowering of one well minimum relative to the other.

A sufficiently strong field can make one configuration unstable. The critical field at which this occurs is the one for which the energy well curvature for that configuration becomes zero. This situation is sketched in Fig. 1.15. In this case, any fluctuation will cause the moment to begin a precession trajectory and dissipation will bring the moment to rest in the lower energy, stable orientation.

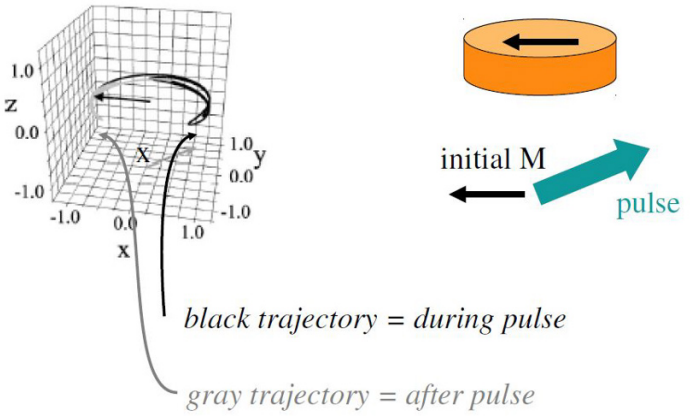

Fig. 1.16 Trajectory of a single domain elliptically shaped particle. After [19] (Used with permission.) Shape anisotropies align the magnetization in plane along the major axis. A static field is applied opposite to the initial magnetization. A pulsed field is applied at an oblique angle to the moment, causing a precessional reversal

1.6.1.1 Field driven precessional reversal

The approximation of a single domain particle is quite severe, but does serve to illustrate general features observed in experiment. Most importantly, it allows for a simple analysis using torque equations wherein the magnetization is replaced by a single block vector representing the instantaneous orientation of the particle's magnetization. An example is shown in Fig. 1.16.

An elliptical dot of soft material is modelled by a single block spin. The geometry in used to define an easy direction in the plane: Shape anisotropies align the magnetization in plane along the major axis, and are represented by uniaxial anisotropies in the effective fields. A static field is applied opposite to the initial magnetization. A pulsed field is applied at an oblique angle to the moment, causing a precessional reversal. The length of the pulse is greater than the relaxation time. Dynamics is modelled by numerically integrating the Landau-Lifshitz equations with Landau damping. The tip of the magnetization vector is traced over the course of the precession. The highly elliptical precession is due to the strong in-plane shape anisotropy.

The success of creating reversal depends sensitively on pulse field duration, magnitude and orientation. Results are shown in Fig. 1.17 for a pulse field that is much shorter than the characteristic relaxation time [19]. A phase diagram is shown where the axes give the orientation and magnitude of the pulse field in a polar plot. The grey shaded regions are ones which lead to reversal, whereas the unshaded areas leave the moment in its initial direction.

1.6.1.2 Thermally driven reversal

Thermal fluctuations can also serve to drive reversal. In Néel's fluctuation model, one imagines that a moment experiences instantaneous effective magnetic fields that are random in orientation and magnitude, with a distribution that depends upon temperature. This is described by a random vector field $\mathbf{h}_f$ included in the torque equations of motion.

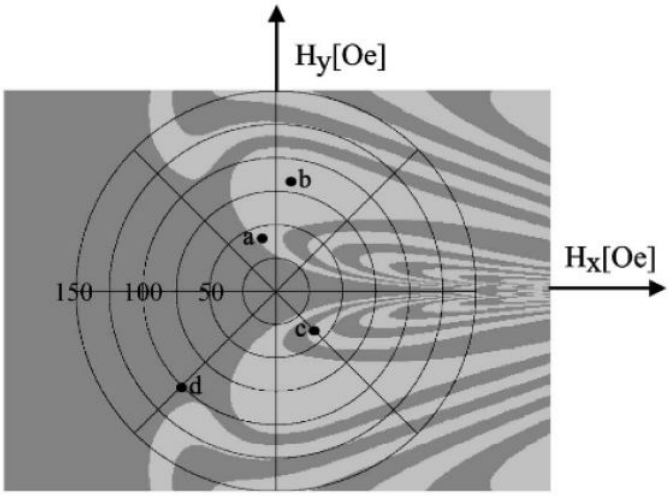

Fig. 1.17 The success of creating reversal using a pulse much shorter than the characteristic relaxation time depends sensitively on field magnitude and orientation. A phase diagram is shown where the axes give the orientation and magnitude of the pulse field in a polar plot. The grey shaded regions are ones which lead to reversal, whereas the unshaded areas leave the moment in its initial direction. After [19] (Used with permission)

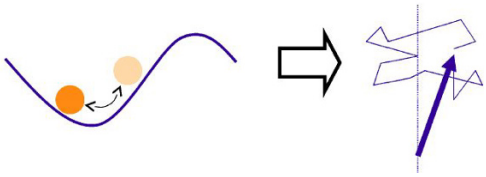

Fig. 1.18 Schematic of thermally driven reversal in a two state model. Some fluctuations are able to drive the magnetization over the barrier

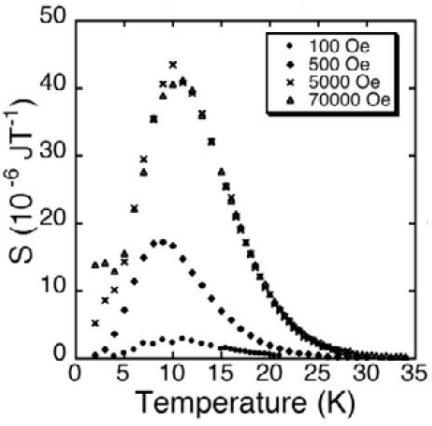

Fig. 1.19 Energy barrier determination for an ensemble of FePt nanoparticles. The distribution is proportional to the magnetic viscosity divided by temperature. After [20] (Used with permission)

Fluctuations can occur on very short timescales in this model, leading to discontinuous changes in the trajectory during otherwise precessional dynamics. A sketch is given in Fig. 1.18. In terms of the two state potential well model, there is a probability that some thermal fluctations will lead to precession that takes the magnetization across the barrier with a final orientation in the opposite direction.

On average, it is possible to construct an estimate of the reversal rate based on the statistics of the fluctuations. Details of a full calculation are complex, but the resulting form is relatively simple

$$\frac{1}{\tau} = f_o \mathrm{e}^{-\frac{\varepsilon}{k_B T}} \ , \tag{1.85}$$

where ε is the barrier "activation" energy, $k_B T$ is the thermal energy at temperature T , and f_o is an "attempt" frequency. The attempt frequency can be

thought of as a measure of the number of ways the magnetic system can fluctuate in such a way as to lead to reversal.

In the Stoner model, the activation energy is estimated for a simple single domain particle from an energy of the form

$$E = V\left(-H_a M_S \cos\theta + K\sin^2\theta\right) , \tag{1.86}$$

where V is the volume and θ is an angle taken relative to a unixaxial anisotropy axis. The activation energy in this model is the energy of the energy maximum at $\theta = \pi/2$. Then $\varepsilon = VK + [H_a M_S/(2K)]^2$.

Reversal in an ensemble of particles is sometimes considered as a chemical rate problem where concentrations of up and down oriented particles are denoted by $n_\uparrow$ and $n_\downarrow$. The rate equations are

$$\frac{\mathrm{d}n_\uparrow}{\mathrm{d}t} = W_{\downarrow\uparrow} n_\downarrow - W_{\uparrow\downarrow} n_\uparrow \tag{1.87}$$

$$\frac{\mathrm{d}n_\downarrow}{\mathrm{d}t} = W_{\uparrow\downarrow} n_\uparrow - W_{\downarrow\uparrow} n_\downarrow . \tag{1.88}$$

Here, transition probabilities $W_{\sigma\sigma'}$ are defined for processes that convert a spin of orientation σ to a spin of orientation σ'. Conservation of particles means that $n_\uparrow + n_\downarrow = 1$ and the magnetization is related to the difference $m(t)$ between concentrations. One finds

$$m(t) = n_\uparrow - n_\downarrow = m(0)\mathrm{e}^{-\Gamma t} , \tag{1.89}$$

where $m(0)$ is a constant determined by the initial conditions, and the relaxation time is defined as $\Gamma = 1/\tau$.

A distribution of relaxation times, $P(\Gamma)$ is taken into account by writing

$$m(t) = m(0)\int P(\Gamma)\mathrm{e}^{-\Gamma t}\mathrm{d}\Gamma . \tag{1.90}$$

In a single process approximation, $\exp(-\Gamma t) \approx 1 - \Theta(t - 1/\Gamma)$. The integral in (1.90) simplifies in this case. Using $P(\Gamma) = P(\varepsilon)\,|d\varepsilon/d\Gamma|$ to convert to an energy barrier distribution, one obtains

$$\frac{\mathrm{d}m}{\mathrm{d}t} \sim -\frac{k_B T}{t} P\left(\varepsilon = k_B T \ln(t/\tau_o)\right) , \tag{1.91}$$

where the time $\tau_o = 1/f_o$ is the inverse activation frequency.

The result represented by (1.91) allows the experimental measure of energy barrier distributions by varying temperature and time. The barrier distribution can be accessed by defining a "viscosity" parameter S defined as

$$P(\varepsilon = k_B T \ln(t/\tau_o)) \approx \frac{1}{m(0)k_B T}\left(-t\frac{\mathrm{d}m}{\mathrm{d}t}\right) = \frac{S}{m(0)k_B T}\,. \tag{1.92}$$

One then plots $S/k_B T$ as a function of temperature to obtain a plot of the barrier distribution. An example of results from this procedure is shown in Fig. 1.19 where S was obtained from an ensemble of FePt particles measured using SQUID magnetometry [20]. Note that the accuracy of this method depends on measurements of the magnetization over very large time scales due to the lograthmic dependence of P on time.

1.6.2 Domain Walls and Magnetization Processes

The reversal process described for a single domain particle in reference to Figs. 1.14 and 1.15 pretained specifically to a magnetic system with two degrees of freedom, corresponding to the two angles used to specify the instantaneous orientation of the magnetic moment. This picture can be generalized to macroscopic magnetic systems with many degrees of freedom corresponding to the orientation of the spatial and time varying magnetization.

Instead of a simple two state system, one then needs to consider an energy landscape with many wells and barriers. Reversal then corresponds to a path through the energy landscape that navigates across saddle points between minima in a landscape controlled by the many degrees of freedom associated with non-uniform magnetic order.

1.6.2.1 Characteristic Lengths

In consequence, magnetization processes in large systems can be complex with new phenomena appearing. How large does a system need to be? A characteristic length is

$$L_{ex} = \sqrt{\mu_o A/M_S^2}\,, \tag{1.93}$$

which is a measure of the distance over which magnetic order can vary. In exchange coupled magnets, deformation of otherwise uniform magnetic order incurs additional exchange energy, and if compared to magnetostatic energy as in (1.93), one can define an "exchange" length below which one would expect uniformly ordered magnetic moments.

Magnetocrystalline anisotropy creates preferred directions for magnetic moments. Different and incompatible orientations can be degenerate in energy, and a large enough system can support multiple orientations. Regions of different orientation will be separated by boundary walls, in much the way that different thermodynamic phases in other many body systems can be separated by phase boundary wall. A comprehensive discussion of domain and wall structure is given by [21].

A characteristic length for this type of magnetic phase separation is called a domain wall length

$$\lambda = \sqrt{A/K}\,. \tag{1.94}$$

This ratio of exchange to anisotropy defines a length over which magnetization can deform across a hard direction. Only ferromagnetic systems are considered for the remainder of this section, although many of the ideas and concepts carry over into multisublattice magnets.

1.6.2.2 Nucleation and Growth of Domains

Consider a ferromagnetic film much thinner than either of the lengths L_{ex} or λ . Magnetic nonuniformities will then occur across the film plane, but not the film thicknesses, at least for temperatures away from the critical point. For definiteness, consider also a strong out of plane oriented uniaxial anisotropy so that the magnetization orients spontaneously perpendicular to the film

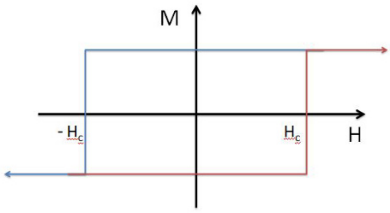

Fig. 1.20 Sketch of average magnetization during an adiabatic field driven reversal

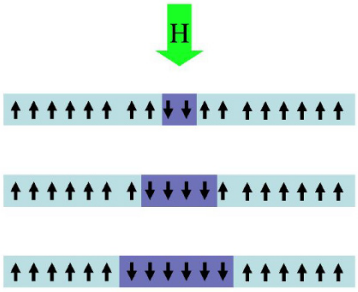

Fig. 1.21 Illustration of domain nucleation. Initially the magnetization is saturated in an easy direction. A magnetic field is applied in the opposite direction, and a small domain can nucleate and grow in size

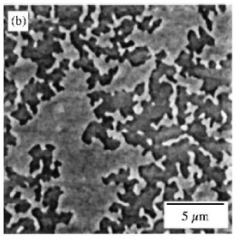

Fig. 1.22 Example of domain structure nucleated in TbFeCo by a sequence of short pulsed fields. The image was taken using a magneto-optical microscope [22]

plane. Note: If the anisotropy is large enough, λ approaches the length of a lattice spacing which is the minimum width of a domain wall. The system then approximates an Ising magnet which is the theoretical construct for a two state magnetic system.

The magnetic film is assumed to be able to exchange heat energy freely with a reservoir (such as a substrate). Now suppose that the magnetization is aligned by a large magnetic field applied along the film normal. Suppose now that the field is now reduced in magnitude slowly, so that the magnetization can respond adiabatically. In a system free from defects or large thermal fluctuations, the magnetization will remain pefectly aligned as the field is reduced to zero and reversed.

It is only until some coercive field $-h_c$ is reached that magnetization can reverse. In a single domain particle at zero temperature, this field corresponds to the field at which the original state becomes unstable and the activation barrier is removed. At finite temperatures, thermal fluctuations can overcome the activation energy barrier (within a time scale set by the experiment) at a field less than the zero temperature coercive field. Once reversal is accomplished, the magnetization aligns along the applied field direction. The aver-

age magnetization for this process is sketched in Fig. 1.20 by the path from positive to negative fields. If now the field is again reduced in magnitude and reversed, the magnetization follows the lower path from negative to positive fields, changing sign to align with the field at $+h_c$.

In an extended film, the change in magnetization orientation at the coercive fields typically begins with the nucleation of domains of reversed magnetization. The process is sketched in Fig. 1.21. Nucleation occurs with a competition between two energies: there is an energy gained by aligning some volume V with the applied field: $E_{Zeeman} = -\mu_o M_S V H_a$. There is an energy cost per area σ_{DW} of forming a domain wall boundary around this volume. If the bounded area is $\mathscr{A}$, then the domain can form when the energies $E_{Zeeman} + \sigma_{DW}\mathscr{A}$ is minimized. This defines a critical size for the domain, given by the ratio $\sigma_{DW}/(\mu_o M_S H_a)$.

An example of a domain structure nucleated in a FeTbCo thin film is shown in Fig. 1.22 [22]. This image was made using a magneto-optical microscope, and the domain pattern is the result of first saturating the magnetization out of plane, and then applying a sequence of small field pulses to nucleate reversal. Several domains nucleate, and then grow in size. The image is taken after several domains have coalesced, thus resulting in a complex pattern of connected regions.

Domains typically nucleate at magnetic or structural defects in a material. Domains grow through motion of domain walls, and the walls themselves can be pinned at defects. This competition between domain wall nucleation and motion results in coercivity and hysteresis, and is strongly dependent on time, temperature, and structural details of the material.

1.6.2.3 Domain Wall Motion in the Creep and Viscous Regimes

As noted earlier, magnetic domain walls are examples of thermodynamic phase boundary walls. They are configurational (topological) excitations of the uniform magnetized ground state, and can be modelled using micromagnetics. Quite often a useful qualitative description can be constructed by approximating the walls as elastic lines with a characteristic width and energy per area.

Some analytical models can be constructed simply in one dimension. These provide insight into the behaviour and properties of domain walls in general, and we review some of the essentials here. A simple model begins with exchange and anisotropy energy and a wall in one dimension

$$E = \int \left[A \left(\frac{\partial u(x)}{\partial x} \right)^2 - K u(x)^2 \right] \mathrm{d}x \,, \tag{1.95}$$

where $u(x) = M_z/M_S$, a normalised component of the magnetization profile. Note that there are two ways to obtain this projection $u(x)$. The magnetization can rotate around the x axis in a Bloch wall configuration, or the magnetization can rotate through the $x-z$ plane in a planar Néel type wall configuration. In the case of the latter, uncompensated magnetic poles exist in the wall, and additional contributions from dipolar energies modify the wall profile and energy. Description of these contributions can be obtained using more advanced approaches or numerical micromagnetics.

The energy of (1.95) can be minimized for a domain wall excitation by first constructing a Euler-Lagrange equation for the integrand. Writing $u(x) = \cos(\theta(x))$, this is of the form

$$A \frac{\partial^2 \theta(x)}{\partial y^2} + K \sin^2(\theta(x)) = 0 \,. \tag{1.96}$$

One solution describes a soliton centered at $x = 0$ with profile parametrized by $\theta(x)$

$$\cos(\theta(x)) = \tanh \left[\frac{x}{\sqrt{A/K}} \right] \,. \tag{1.97}$$

The width λ can be defined from $\lambda = \sqrt{A/K}$ and represents a competition between the exchange, which tends to align moments relative to one another, and anisotropy, which tends to align magnetization relative to a direction in the material. Substitution of this solution into the energy of (1.95) results in the energy per length

$$\sigma_{DW} = \sqrt{4AK} \,. \tag{1.98}$$

In materials with small anisotropy, wall like structures will be strongly modified by dipolar energies, and the above model is less applicable. High anisotropy materials produce narrow domain walls which more closely resemble the above model. In these materials, walls can move freely if no pinning sites or other defects exist.

Motion of a domain wall is still governed by torque equations, and involves precession. A wall will move under the influence of magnetic field, for example, to a first approximation without changing its profile. Dissipation

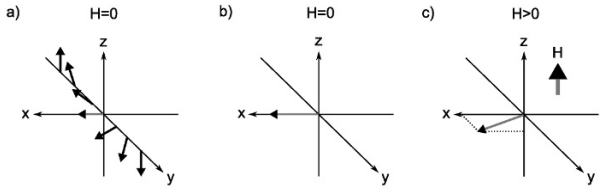

Fig. 1.23 Moments inside a Bloch wall at rest will rotate in a plane normal to the wall axis. In motion, the plane of rotation is tilted so that a component of the moments lies along the wall axis [23]

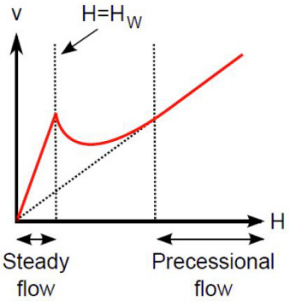

Fig. 1.24 Walker breakdown occurs when magnetostatic charges built up within a propagating wall drive internal dynamics. The onset occurs at a critical driving field, and drastically modify the wall velocity [25]

Fig. 1.25 Motion of a domain wall in the creep regime is governed by avalanche dynamics. Depinning from one site can lead to a cascade of other depinnings that reverse an area of magnetization

will determine the speed, and the wall will move at a constant rate determined by the field magnitude. The rate, or speed v_{DW} , will be determined by the dissipated power averaged over time (the overbar stands for time-averaging)

$$v_{DW} \propto \alpha \int \overline{|\mathbf{M} \times H_{eff}|^2} \mathrm{d}x \,. \tag{1.99}$$

This is a terminal velocity. The wall speed will be linear in the applied field magnitude and proportional to the damping constant.

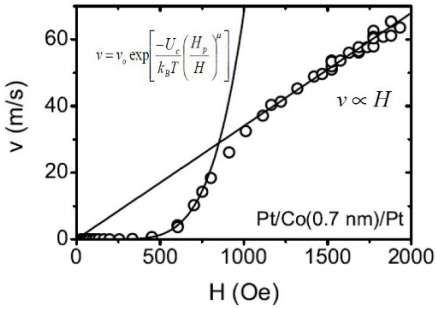

Fig. 1.26 Measured velocities for domain wall creep in a 0.5 nm thick Co film. The lines are fits to the data in the creep and viscous regimes [25]

We note here also an effect that can occur for large speeds and driving fields. Taking into account some modifications of the profile, one finds that the moments in a Bloch wall will tilt slightly out of the plane of the wall. This is shown schematically in Fig. 1.23. This means that a component of the magnetization will appear along the wall axis, leading to uncompensated magnetic charge. As a result there will be a magnetostatic contribution to the wall energy. In a nanowire, the magnitude of the tilt will also depend on the shape of the wire through demagnetizing factors. At high fields, this angle will increase and can lead to an instability known as Walker breakdown. In this type of motion, internal oscillations appear that result in a change the wall velocity. The corresponding effects on the field dependence of the wall velocity are illustrated in Fig. 1.24. Internal oscillations set in at a critical field H_W, and at higher fields the velocity is strongly reduced and wall motion involves precession within the wall itself. Shape anisotropies in nanostructures can affect the onset of criticality, through shape anisotropies [24].

Motion at low fields in the presence of pinning can lead to a phenomena known as “creep”. Suppose that a narrow wall exists in a planar ferromagnet with a distribution of point defects that can pin a wall. Such a site might be associated with a local variation in anisotropy or exchange, for example, which lowers the magnetic energy if intersected by a wall. The wall energy depends upon its length, and there will be a competition between wall and pinning energies that determine the wall configuration.

Application of a magnetic field will exert a pressure on the wall and can cause an adjustment of the configuration as the wall again seeks to minimize its length against the constraint of intersecting pinning sites. Each pinning site itself represents a potential energy well for a wall to sit in, and so ther-

mal fluctuations can cause portions of the wall to depin and move to a new pinning site. However depinning from one site may increase the probability of depinning from a nearby site, thereby leading to an avalanche dynamics, as depicted in Fig. 1.25.

In this way, motion of the wall occurs in a series of discrete jumps associated with depinning avalanches. This is also known as Barkhausen noise in that each jump corresponds to the reversal of an area of magnetization and change in the net magnetization.

A description of creep as avalanche dynamics provides a useful means of determining the average velocity of a wall. An applied field of sufficient strength will overcome all barriers and the wall will move linearly with field as in the viscous regime discussed above. At zero temperature, thermal fluctuations will not play a role, and there will be a critical value H_{depin} for the applied field that defines a depinning transition. At this field, any magnitude of avalanche becomes possible, and this insight allows one to define scaling relations for the size of the avalanches. Scaling arguments can then be used to define a depinning energy as the difference between elastic and applied field Zeeman energies

$$E_{elastic} - E_{Zeeman} = E_{depin} \approx U_C \left(\frac{H_{depin}}{H_a} \right)^{\frac{2\zeta - 2 + D}{2 - \zeta}} . \tag{1.100}$$

The exponent ζ in (1.100) and other critical exponents can be derived from renormalization group methods, and D is the dimensionality. The constant U_C is a measure of the pinning potential distribution. The energy E_{depin} represents a barrier to motion of the domain wall in analogy to the activation energy presented earlier in the context of single particle reversal. One can then define an average displacement for a wall overcoming this energy, and assign a characteristic time τ_o to the process. This then allows definition of a speed in the creep regime

$$v_{creep} \approx \frac{\xi}{\tau_o} \exp \left[- \frac{U_C}{k_B T} \left(\frac{H_{depin}}{H_a} \right)^{\mu} \right] , \tag{1.101}$$

where the exponent μ is calculated to be $1/4$ for films thin enough to be considered two dimensional.

An example of measured creep motion for a specially constructed thin 0.5 nm thick Co film is shown in Fig. 1.26 [25]. The measurements were made using magneto-optical microscopy, with motion of the wall created by a pulsed magnetic field. The sample was held at room temperature. Velocities were de-

termined by measuring the distance travelled for a known duration pulse. The straight line is a fit to the wall motion in the viscous regime. The low field data is fit with the creep law (1.101) using $\mu = 0.25$. The transition region between creep and viscous motion lies between 500 and 1200 Oe. A recent summary of creep dynamic experiments can be found in [23].

1.6.2.4 Summary

A summary of concepts and ideas useful for an understanding of measurable phenomena in thin film and nanostructured magnetic materials has been provided. Materials magnetism begins with electronic spin and chemical bonds. Beginning with the base definitions of magnetic moment and its relation to angular momentum, mechanisms were discussed for long range ordering based on electronic orbital overlap in insulators, and electronic band structure in metals.

Equally important to the existence of a magnetically ordered ground state, is the nature of excitations about this ground state. Correlations between spin fluctuations define the lowest energy excitations in ordered magnetic systems, and it was shown how these can be understood by analogy to the quanta of harmonic oscillations associated with vibrations in crystals. A phenomenological model of magnetic ordering and excitations is also described, and key parameters defined in terms of symmetries allowed by the local atomic environment.

The thermodynamic view of magnetic states and configurations is particularly useful for understanding a variety of phenomena, and also for many applications. Here the focus has been on mechanisms for magnetic reversal and coercivity and the concepts of magnetic domain walls and domain wall mobilities are discussed.

The scope of the discussion has been limited to introductory ideas, neglecting a number of very interesting and technologically important developments of recent years. In particular, there is a wealth of new knowledge accumulated regarding electron transport and spin torque transfer that has not been presented. These topics themselves fill several reviews and fall well outside the scope of this brief introduction.

Before closing, there is one other area that is currently developing very quickly. As modern lithographic techniques advance, so to is the ability to define magnetic elements with nanoscale precision in two and three dimensional arrays. The dimensions and geometry of the arrays can be defined such that

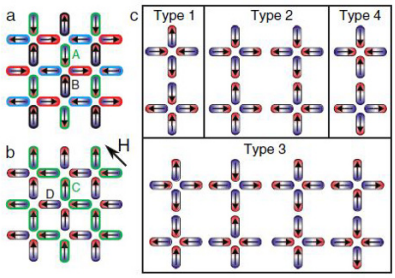

Fig. 1.27 Geometry for a square artificial spin ice array. Configurations can be characterized by arrangements of magnetic poles at vertices. Sixteen different vertex configurations are possible. After [26] (Used with permission)

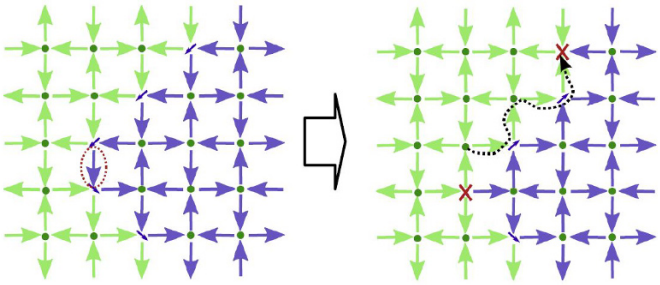

Fig. 1.28 Sketch of a square artificial magnetic ice array. The arrows indicated the domain magnetization of individual elements. Two array ground states are shown with a boundary indicated by the small arrows at vertices. Domain growth occurs through an avalanche along the boundary triggered by a single element reversal at an array domain corner. After [27] (Used with permission)

the individual element interact strongly through, for example, stray dipolar magnetic fields.

These arrays are intriguing as they represent new classes of "artificial" magnetic materials. The materials are artificial in that the interaction strengths can be controlled to a large extent, and response to thermal fluctuations engineered. These systems, in various geometries, have been realized experimentally and typically the element sizes have been chosen to around 200 nm in length, and usually of a soft material such as FeNi. The larger sizes approximate single domain particles and are stable against thermal fluctuations.

A particularly interesting class of arrays use geometry to create frustration in what are called "artificial spin ices". It is useful in these systems to

think of the magnetic orientations at vertices. There are sixteen possible vertex configurations in a square spin ice, and they can be ranked in terms of their corresponding energies due to interactions. There are four distinct energies, allowing for a defintion of four vertex classes. The square ice geometry and corresponding vertex classes are shown in Fig. 1.27 [26].

Reversal of elements accomplished through applied fields, and generally involve a cascade of elemental reversals due to strong inter-element interactions. An example of a spin configuration is sketched in Fig. 1.28 for a square lattice [27]. The lattice is designed to encourage the magnetic elements to align such that the net magnetization is zero, as in a multisublattice antiferromagnet. The large arrows indicate the orientation of element magnetizations, and in this geometry two incompatible ground states are possible for the array. Each ground state is characterized by two arrows in and two arrows out, in analogy to the polar bonds in water ice that obey a similar "ice" rule for the lowest energy configuration.

The arrangement shown in Fig. 1.28 shows the boundary between two neighbouring array ground states. The boundary carries a net magnetic moment, as indicated by the small arrows. Growth of a domain occurs by motion of the boundary. Motion of the boundary occurs via reversals of element magnetizations. The first element to reverse is at a corner of the array domain, and leads to a cascade of other element reversals in a one dimensional avalanche. This avalanche may be triggered by an external field or, if the elements are small enough, by thermal fluctuations.

This example illustrates that the concepts and models developed for continuous films and materials have extensions and applicability to a new class of magnetic systems. The potentials to define key characteristic lengths and energies through nanoscale design allow one to create and engineer new properties and functionalities. The phase space of possibilities is extraordinarily large, and to date only a few examples have been examined. The history of magnetism is one punctuated by the discovery of new and useful phenomena with each advance in materials technology, suggestive of a very interesting future ahead indeed.

References

1. D. C. Mattis, *The Theory of Magnetism* (Harper & Row, 1965)
2. R. M. White, *Quantum Theory of Magnetism* (Springer-Verlag, 1983)

3. J. M. D. Coey, *Magnetism and Magnetic Materials* (Cambridge University Press, 2010)
4. C. Kittel, *Introduction to Solid State Physics*, 8th edn. (John Wiley & Sons, 2004)
5. A.H. Morrish, *Physical Principles of Magnetism* (Wiley-IEEE Press, 2001)
6. V. Gunawan and R.L. Stamps, J. Phys.: Cond. Matter, **23**, 105901 (2011)
7. M.A. Ruderman and C. Kittel, Phys. Rev. **96**, 99 (1954)
8. F.J. Dyson, Phys. Rev., **102**, 1217 (1956)
9. A. I. Akhiezer , V. G. Baryakhtar, S. V. Peletminskii, *Spin Waves* (North-Holland, 1968)
10. Z. S. Borovik-Romanov and S. K. Sinha, *Spin waves and Magnetic Excitations* (Elsevier, 1988)
11. S. O. Demokritov, *Magnonics: From Fundamentals to Applications* (Springer, 2012)
12. D. D. Stancil and A. Prabhakar, *Spin Waves: Theory and Applications* (Springer, 2009)
13. A. Gurevich, G. A. Melkov, Magnetization Oscillations and Waves (CRC Press, 1996)
14. L. Landau and L. Lifshitz, Physik Z. Sowjet. **8**, 153 (1935)
15. T. L. Gilbert, Phys. Rev. **100**, 1243 (1955)
16. M. Sparks, *Ferromagnetic-relaxation theory* (McGraw-Hill, 1964)
17. V. S. L'Vov, *Wave Turbulence Under Parametric Excitation: Applications to Magnets* (Springer, 1994)
18. G. Bertotti, I. D. Mayergoyz, C. Serpico, *Nonlinear Magnetization Dynamics in Nanosystems* (Elsevier, 2009)
19. M. Bauer, J. Fassbender, B. Hillebrands, R.L. Stamps, Phys. Rev. B **61**, 3410 (2000)
20. R. O. Fuller, G.A. Koutsantonis, R.L. Stamps, J. Phys.: Cond. Matter. **21**, 124203 (2009)
21. A. Hubert and R. Schäfer, *Magnetic Domains: The analysis of Magnetic Microstructures* (Springer-Verlag, 1998)
22. R.C. Woodward, K.L. Livesey, R.L. Stamps, J. Magn. Magn. Mater. **272-276**, E531(2004)
23. P.J. Metaxas, Solid State Physics **62**, 75 (2011)
24. A. Mougin, M. Cormier, J.P. Adam, P.J. Metaxas and J. Ferré, Europhys. Lett. **78**, 57007 (2007)
25. P. Metaxas, J.-P. Jamet, A. Mougin, M. Cormier, J. Ferré, V. Baltz, B. Rodmacq, B. Dieny, and R. L. Stamps, Phys. Rev. Lett. **99**, 217208 (2007)
26. Z. Budrikis, J. P. Morgan, J. Akerman, A. Stein, Paolo Politi, S. Langridge, C. H. Marrows, and R. L. Stamps, Phys. Rev. Lett. **109**, 037203 (2012)
27. Z. Budrikis, P. Politi, R. L. Stamps, New J. Phys. **14**, 045008 (2012)